The International Journal of Robotics Research

http://ijr.sagepub.com

Computation and Graphical Characterization of Robust Multiple-Contact Postures in Two-Dimensional Gravitational Environments

Yizhar Or and Elon Rimon

The International Journal of Robotics Research 2006; 25; 1071
DOI: 10.1177/0278364906072038

The online version of this article can be found at:
http://ijr.sagepub.com/cgi/content/abstract/25/11/1071

Published by:
SAGE
http://www.sagepublications.com

On behalf of:
MM
Multimedia Archives

Yizhar Or
Elon Rimon

Dept. of Mechanical Engineering
Technion, Haifa, Israel 32000
elon@robby.technion.ac.il

Computation and Graphical Characterization of Robust Multiple-Contact Postures in Two-Dimensional Gravitational Environments

Abstract

This paper is concerned with computation and graphical characterization of robust equilibrium postures suited to quasistatic multi-legged locomotion. Quasistatic locomotion consists of postures in which the mechanism supports itself against gravity while moving its free limbs to new positions. A posture is robust *if the contacts can passively support the mechanism against gravity as well as disturbance forces generated by its moving limbs. This paper is concerned with planar mechanisms supported by frictional contacts in two-dimensional gravitational environments. The kinematic structure of the mechanism is lumped into a rigid body $\mathcal{B}$ having the same contacts with the environment and a variable center of mass. Inertial forces generated by moving parts of the mechanism are lumped into a neighborhood of wrenches centered at the nominal gravitational wrench. The robust equilibrium postures associated with a given set of contacts become the center-of-mass locations of $\mathcal{B}$ that maintain equilibrium with respect to all wrenches in the given neighborhood. The paper formulates the computation of the robust center-of-mass locations as a linear programming problem. It provides graphical characterization of the robust center-of-mass locations, and gives a geometric algorithm for computing these center-of-mass locations. The paper reports experiments validating the equilibrium criterion on a two-legged prototype. Finally, it describes initial progress toward computation of robust equilibrium postures in three dimensions.*

The International Journal of Robotics Research
Vol. 25, No. 11, November 2006, pp. 1071-1086
DOI: 10.1177/0278364906072038

KEY WORDS—legged locomotion, frictional contact, robust equilibrium stances

1. Introduction

Multi-legged robots capable of autonomous quasistatic locomotion are becoming progressively more sophisticated. Developers of legged robots strive to achieve stable locomotion on uneven terrains such as staircases (Hirai et al. 1998), complex posture changes such as sitting and standing up (Yokokehji et al. 2002), cargo lifting (Omata et al. 2002), and climbing (Bretl et al. 2003; Madhani and Dubowsky 1992). Quasistatic locomotion can be characterized as a series of postures in which the mechanism supports itself against gravity while moving its free limbs to new positions. For instance, the 3-legged robot shown in Figure 1 moves with a gait of 3-legged phases interleaved with 2-legged phases where it lifts a leg to a new position (Rimon et al. 2001). In order to achieve autonomous locomotion of such robots over uneven terrains, one needs basic tools for selecting postures that can passively support the mechanism against gravity while allowing motion of its free limbs according to task specification. The paper introduces the notion of posture robustness which captures this basic need.

The paper focuses on planar mechanisms supported by frictional contacts in a two-dimensional gravitational environment. As a first step, we lump the complex kinematic structure of the mechanism into a single rigid body $\mathcal{B}$ having the same contacts with the environment and a variable center of mass. The feasible equilibrium postures associated with a given set of contacts and the nominal gravitational wrench correspond

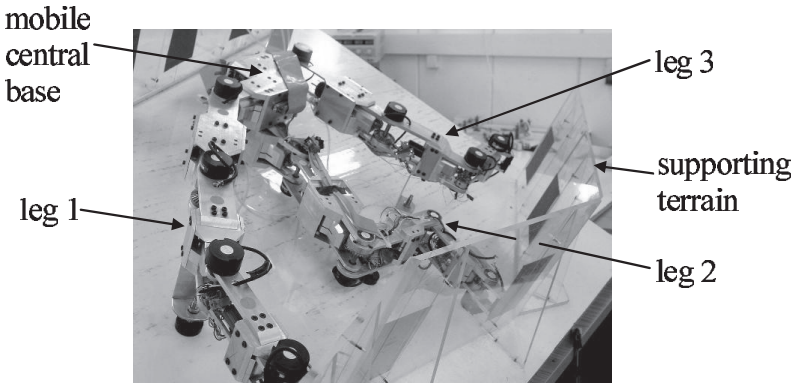

Fig. 1. A three-legged robot moving in a two-dimensional gravitational environment (the mechanism is supported by frictionless air bearings against the inclined plane).

to center-of-mass locations of $\mathcal{B}$ that guarantee a feasible equilibrium stance for the same contacts. However, the mechanism is additionally subjected to inertial forces generated by its moving parts. We lump these forces into a neighborhood of disturbance wrenches (i.e., forces and torques) centered at the nominal gravitational wrench. Under this reduction, a stance of $\mathcal{B}$ is *robust* if the contacts can passively resist the entire wrench neighborhood. Based on this notion of robustness our objective is as follows. Given a k-contact stance of $\mathcal{B}$ and a neighborhood of disturbance wrenches, we wish to identify the *robust equilibrium region* defined as all center-of-mass locations of $\mathcal{B}$ at which the contacts can passively resist the wrench neighborhood.

Relationship to prior work. Stance stability received considerable attention in the early multi-legged locomotion literature (Marhefka and Orin 1997; McGhee and Frank 1968). More recent papers discuss stance stability in humanoid robots (Hirai et al. 1998; Kuffner et al. 2001; Vukobratovic and Borovac 2004; Yokokohji et al. 2002). Mason et al. (1995) introduced the idea of lumping the kinematic structure of a mechanism into a rigid body having the same contacts with the environment and a variable center of mass. They identify the stable stances of a body supported by frictionless contacts in two and three dimensions. Taking friction into account, Madhani and Dubowsky (1992) as well as Bretl et al. (2003a, b) developed locomotion planners for three-legged climbing robots. These papers plan the mechanism's postures using its full configuration space. While this approach is justifiable for extremely simplified robots, a three-legged robot such as the one shown in Figure 1 has twelve actuated joints and three unactuated degrees of freedom at its central base (Rimon, Shoval, and Shapiro 2001). By focusing on the contacts and center-of-mass position, planning of the mechanism's postures requires only a reduced set of parameters. The robust equilibrium region introduced in this paper provides a basic posture-selection tool for such reduced planners.

Let us next discuss the grasping literature. Typical grasping systems assume full control of the contact forces. In these systems *force closure* captures the ability of the fingers to actively resist any external wrench acting on the grasped object (Fen et al. 1996; Liu et al. 2002; Schlegl et al. 2001; Xu et al. 2004). Multi-limb locomotion based on force closure is useful in tunnel-like environments where the mechanism can brace itself against opposing walls (Greenfield et al. 2005; Shapiro and Rimon 2003). However, legged locomotion involves contacts that can typically balance only a neighborhood of wrenches about the gravitational force. Moreover, legged mechanisms are supported by *passive* contacts that can only react to applied wrenches. The notion of posture robustness can thus be interpreted as force closure for passive contacts. Legged locomotion is more related to passive grasping applications such as whole arm manipulation[1] (Erdmann 1998; Mirza and Orin 1994; Omata and Nagata 2000; Trinkle et al. 1994, 1995), fixturing (Wang 2001; Yoshikawa 1999), and object recognition (Kriegman 1994). An especially relevant work by Erdmann et al. (1998) considers the feasible center-of-mass positions of objects held in frictional 2-contact stances by a palm manipulator. Note, however, that a multi-legged mechanism can control the gravitational wrench by varying its center-of-mass position. The latter possibility is analogous to pushing applications, where an object is manipulated in a planar environment by a pushing force (Lynch and Mason 1996). A graphical moment-labelling technique developed for these applications (Brost 1991; Mason 1991) can be adapted to the stances considered here. We offer a

1. In whole arm manipulation an object is manipulated by one or more articulated mechanisms that are allowed to establish multiple mid-link contacts with the manipulated object (Bicchi 2000).

complementary technique which is specifically designed for depicting the robust center-of-mass locations.

Finally, this paper focuses on robust equilibrium stances that can passively resist neighborhoods of disturbance wrenches. Two additional criteria that should be incorporated into future quasistatic locomotion planners are as follows. The first is associated with ambiguity incurred by rigid-body dynamics in the presence of frictional contacts (Dupont and Yamajako 1994; Lotstedt 1981; Mason and Wang 1988). One must ensure that a feasible equilibrium is dynamically non-ambiguous (Lynch 1992), or *strongly stable* (Pang and Trinkle 2000). Second, one must ensure that a candidate equilibrium posture is dynamically stable with respect to position-and-velocity perturbations. This classical type of stability must account for contact breakage and slippage. While initial progress is reported for specific scenarios (Ghasempoor and Sepehri 1995; Harada et al. 2003; Papadopoulos and rey 1996), a general stability theory in frictional multi-contact settings is still an active research area.

The structure and contributions of the paper are as follows. The paper first considers center-of-mass positions that give a feasible equilibrium of $\mathcal{B}$ under the influence of a single external wrench. Section 2 formulates this region as a linear programming problem. Section 3 provides its graphical characterization and a potentially faster line-sweep algorithm for its computation. The main result is that the feasible equilibrium region of a general k-contact stance is an *infinite strip* whose position and orientation is determined by the contacts and the external wrench acting on $\mathcal{B}$. The paper next generalizes this result to neighborhoods of disturbance wrenches. Section 4 formulates the robust equilibrium region as a linear programming problem and provides its graphical characterization. The main result in this part of the paper is that the robust equilibrium region of a general k-contact stance is a *parallelogram* whose shape and size is determined by the contacts and the wrench neighborhood. Section 5 reports on experiments validating the analytical equilibrium criterion on a two-legged prototype. Posture robustness is eventually intended for three-dimensional environments. Section 6 establishes that the equilibrium region associated with the nominal gravitational wrench is a three-dimensional *convex vertical prism,* then it summarizes the challenges involved in its computation. The paper concludes with a discussion of the need to augment posture robustness with dynamic as well as strong stability.

2. The Feasible Equilibrium Region

We first introduce basic terminology and define the feasible equilibrium region of a stance. Then we formulate the computation of the feasible equilibrium region as a linear programming problem, and draw two properties useful for its graphical characterization.

2.1. Basic Terminology

Let $\mathcal{B}$ be a planar rigid object with a variable center of mass, which is supported by k frictional point contacts in a two-dimensional gravitational environment. The gravitational force acting at the center of mass of $\mathcal{B}$, denoted f_g, defines the vertical downward direction. The environment is assigned a fixed world frame aligned with the vertical direction, and $\mathcal{B}$ is assigned a body frame with origin at its center of mass. The position of the center of mass of $\mathcal{B}$ in the world frame is denoted x. The contact points are denoted $x_1 \ldots x_k$ (all expressed in the fixed world frame), and the contact forces acting on $\mathcal{B}$ are denoted $f_1 \ldots f_k$. Using this notation, the torque generated by f_i about $\mathcal{B}$'s center of mass is the scalar $\tau_i = (x_i - x)^T J^T f_i$, where $J = \begin{bmatrix} 0 & -1 \\ 1 & 0 \end{bmatrix}$. Assuming Coulomb's friction law, each force f_i must lie in a *friction cone*, denoted $\mathcal{C}_i$, in order to avoid sliding. Let f_i^n and f_i^t denote the normal and tangential components of f_i. Then $\mathcal{C}_i = \{f_i : |f_i^t| \leq \mu f_i^n,\ f_i^n \geq 0\}$ where μ is the coefficient of friction. We also need the following equivalent terminology for $\mathcal{C}_i$. Let C_i^l and C_i^r denote unit vectors along the left and right edges of $\mathcal{C}_i$ (Figure 2(a)). Then the i^{th} friction cone is given by $\mathcal{C}_i = \{f_i^l C_i^l + f_i^r C_i^r : f_i^l, f_i^r \geq 0\}$. The object $\mathcal{B}$ is additionally subjected to a disturbance wrench $(f_d, \tau_d) \in \mathbb{R}^2 \times \mathbb{R}$, where (f_d, τ_d) is expressed with respect to $\mathcal{B}$'s center of mass. Let $\boldsymbol{w} = (f_{ext}, \tau_{ext}) \in \mathbb{R}^2 \times \mathbb{R}$ denote the net external wrench acting on $\mathcal{B}$, then $f_{ext} = f_g + f_d$ such that $\|f_d\| \ll \|f_g\|$. Since f_g generates no torque about x, we have that $\tau_{ext} = \tau_d$.

The equilibrium condition is as follows. Let G_f and G_τ denote the matrices associated with the forces and torques at the contacts:

$$G_f = \begin{bmatrix} C_1^l & C_1^r & \cdots & C_k^l & C_k^r \end{bmatrix}_{2\times 2k}$$
$$G_\tau = -\begin{bmatrix} x_1^T J C_1^l & x_1^T J C_1^r \cdots x_k^T J C_k^l & x_k^T J C_k^r \end{bmatrix}_{1\times 2k}.$$

Let $\boldsymbol{f} = \begin{pmatrix} f_1^l & f_1^r \cdots f_k^l & f_k^r \end{pmatrix}$ denote the $2k$-vector of normal and tangential contacts force components. Then the equilibrium condition is given by

$$\begin{bmatrix} G_f \\ G_\tau \end{bmatrix} \boldsymbol{f} = -\begin{pmatrix} f_{ext} \\ \tau(x) \end{pmatrix} \text{ and } \boldsymbol{f} \geq \vec{0}, \qquad (1)$$

where $\tau(x) = x^T J^T f_{ext} + \tau_{ext}$ is the net torque generated by $\boldsymbol{w} = (f_{ext}, \tau_{ext})$ about the world frame origin. Note that the contact forces are statically indeterminate for $k \geq 2$ contacts. We can now formally define the feasible equilibrium region.

DEFINITION 1. Given a k-contact stance and an external wrench $\boldsymbol{w}$ acting on $\mathcal{B}$, the **feasible equilibrium region** associated with $\boldsymbol{w}$, denoted $\mathcal{R}(\boldsymbol{w})$, is the set of $\mathcal{B}$'s center-of-mass locations for which there exist contact forces $f_i \in \mathcal{C}_i$ $(i = 1 \ldots k)$ satisfying the equilibrium condition (1).

2.2. Computation of the Feasible Equilibrium Region

We show that the feasible equilibrium region is an infinite strip computable as a linear programming problem. As noted

by several authors (Bretl et al. 2003b; Mason et al. 1997), the equilibrium formulation (1) can be interpreted as a collection of linear inequalities in the composite $(\boldsymbol{f}, x)$ space. The following key theorem characterizes the feasible equilibrium region as a pair of linear programs.

THEOREM 1. Let $\mathcal{B}$ be supported by $k \geq 2$ frictional contacts in a two-dimensional gravitational field, and be subjected to a net external wrench $\boldsymbol{w} = (f_{ext}, \tau_{ext})$. If the feasible equilibrium region $\mathcal{R}(\boldsymbol{w})$ is nonempty, it is generically an **infinite strip** parallel to f_{ext} given by

$$\mathcal{R}(\boldsymbol{w}) = \left\{x \in I\!R^2 : \tau_{min} \leq x^T J^T f_{ext} + \tau_{ext} \leq \tau_{max}\right\}, \quad (2)$$

where τ_{min} and τ_{max} are obtained by solving the linear programming problems:

$$\begin{aligned} \tau_{min} &= \min_{G_f \boldsymbol{f} = -f_{ext},\, \boldsymbol{f} \geq \vec{0}} \{-G_\tau \boldsymbol{f}\} \\ \tau_{max} &= \max_{G_f \boldsymbol{f} = -f_{ext},\, \boldsymbol{f} \geq \vec{0}} \{-G_\tau \boldsymbol{f}\} \end{aligned} \quad (3)$$

Proof. The k contacts and external wrench are fixed. Hence the equilibrium and friction constraints take place in a $(2k+1)$-dimensional space whose coordinates are $(\boldsymbol{f}, \tau)$, where τ is the net torque acting on $\mathcal{B}$ with respect to a fixed world frame. Since the constraints in (1) are linear in $\boldsymbol{f}$ and τ, they form a convex polytope in $I\!R^{2k+1}$. For $k \geq 2$ contacts the projection of the $(\boldsymbol{f}, \tau)$-polytope onto the τ-axis is an interval $[\tau_{min}, \tau_{max}]$. Once the interval is computed, its pre-image under the linear mapping $\tau(x) = x^T J^T f_{ext} + \tau_{ext}$ yields an infinite strip parallel to f_{ext} of allowed center-of-mass locations. The projection of the polytope onto the τ-axis is equivalent to the following pair of linear programs in $\boldsymbol{f}$-space. According to (1), $\tau = -G_\tau \boldsymbol{f}$. Hence the extreme values of τ over the $(\boldsymbol{f}, \tau)$-polytope correspond to the minimum and maximum of $-G_\tau \boldsymbol{f}$ over the $\boldsymbol{f}$-polytope: $\{\boldsymbol{f} : G_f \boldsymbol{f} = -f_{ext}, \boldsymbol{f} \geq \vec{0}\}$. These extreme values are τ_{min} and τ_{max} in the linear programs of the theorem. □

Let us make a three comments on the theorem. First, the interval $[\tau_{min}, \tau_{max}]$ captures the range of torques that can be resisted by contact reaction forces satisfying force equilibrium and friction constraints. The feasible equilibrium strip can therefore be written as $\mathcal{R}(\boldsymbol{w}) = \{x : \tau_{min} \leq \tau(x) \leq \tau_{max}\}$. Second, in certain situations τ_{min} or τ_{max} can be unbounded. In these cases $\mathcal{R}(\boldsymbol{w})$ spans a halfplane or the entire plane as demonstrated in Example 1. Third, for a single contact $\mathcal{R}(\boldsymbol{w})$ is a line parallel to f_{ext} and passing through the contact. The strip $\mathcal{R}(\boldsymbol{w})$ associated with $k \geq 2$ contacts degenerates to such a line in the special case where all friction cones point to the same side of f_{ext}, such that one friction cone edge is aligned with f_{ext}.

EXAMPLE 1. Figure 2(a) shows the region $\mathcal{R}(\boldsymbol{w})$ for two contacts with $\mu = 0.3$, using the nominal gravitational wrench $\boldsymbol{w} = (f_g, 0)$. Note that $\mathcal{R}(\boldsymbol{w})$ is a vertical strip spanned by the polygon $\mathcal{C}_1 \cap \mathcal{C}_2$. This observation is part of the full graphical characterization discussed below. Figure 2(b) shows the same stance with $\mu = 2.0$, using the nominal gravitational wrench $\boldsymbol{w} = (f_g, 0)$. In this case τ_{min} and τ_{max} are unbounded and $\mathcal{R}(\boldsymbol{w})$ spans the entire plane. Note that in this case the line segment connecting x_1 and x_2 is contained in the friction cones $\mathcal{C}_1$ and $\mathcal{C}_2$, thus satisfying Nguyen's frictional force closure condition (Nguyen 1988). In general, $\mathcal{R}(\boldsymbol{w}_0)$ is bounded when the friction cones are *upward pointing*, in the sense that $f_i \cdot f_g \leq 0$ for all $f_i \in \mathcal{C}_i$ $(i = 1, 2)$. Indeed, both friction cones are upward pointing in Figure 2(a), while none is upward pointing in Figure 2(b).

2.3. Properties of the Feasible Equilibrium Region

We now describe two structural properties of $\mathcal{R}(\boldsymbol{w})$. The first property will be the basis for the graphical characterization and is stated in the following proposition.

PROPOSITION 1. Let $\mathcal{B}$ be supported by k frictional contacts in a two-dimensional gravitational environment, and be subjected to an external wrench $\boldsymbol{w} = (f_{ext}, \tau_{ext})$. Then $\mathcal{R}(\boldsymbol{w})$ is the convex hull of the pairwise feasible equilibrium regions,

$$\mathcal{R}(\boldsymbol{w}) = \mathsf{conv}\{\mathcal{R}_{ij}(\boldsymbol{w}),\ 1 \leq i, j \leq k\},$$

where $\mathcal{R}_{ij}(\boldsymbol{w})$ is the feasible equilibrium region associated with two contacts x_i and x_j, and conv denotes convex hull.

A proof of the proposition appears in Appendix A. The proposition asserts that $\mathcal{R}(\boldsymbol{w})$ can be computed in terms of the equilibrium strips generated by all pairs of contacts. Since these strips are all parallel to f_{ext}, their convex hull is simply the strip bounded by the leftmost and rightmost edges of the pairwise strips. A second notable property is that $\mathcal{R}(\boldsymbol{w})$ is completely determined by at most *four* out of the k contacts. This observation is stated in the following corollary.

COROLLARY 1. Let $\mathcal{B}$ be supported by $k \geq 4$ frictional contacts in a two-dimensional gravitational environment, and be subjected to an external wrench $\boldsymbol{w} = (f_{ext}, \tau_{ext})$. Let $\mathcal{R}(\boldsymbol{w})$ be the feasible equilibrium region associated with $\boldsymbol{w}$. Then there exist at least $k-4$ contacts that can be removed without affecting $\mathcal{R}(\boldsymbol{w})$.

A proof of the corollary also appears in the appendix. Note that the remaining contacts are non-essential for the purpose of determining the feasible equilibrium region. These contacts may prove important for other purposes, such as contact force minimization over the center-of-mass locations.

EXAMPLE 2. Figure 2(c) shows the region $\mathcal{R}(\boldsymbol{w})$ for six contacts with $\mu = 0.4$, using the nominal gravitational wrench $\boldsymbol{w} = (f_g, 0)$. Computing the vertical strips $\mathcal{R}_{ij}(\boldsymbol{w})$ associated with all possible pairs of contacts, one can see that the leftmost edge is associated with $\mathcal{R}_{13}$ while the rightmost edge is associated with $\mathcal{R}_{56}$. The feasible equilibrium region associated

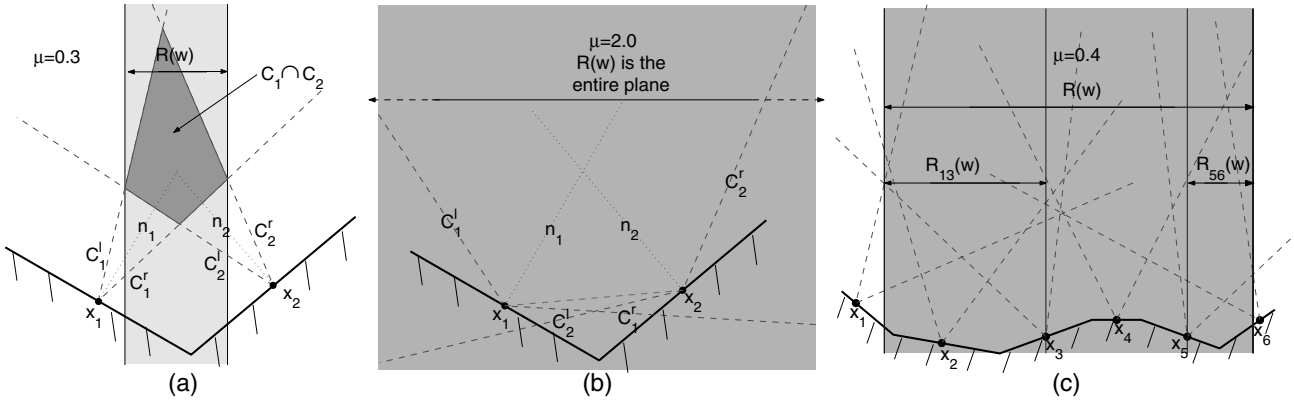

Fig. 2. The feasible equilibrium region $\mathcal{R}(\boldsymbol{w})$ for (a)-(b) two contacts, and (c) six contacts.

with all six contacts is simply the vertical strip bounded by the leftmost and rightmost edges. Moreover, the four contacts x_1, x_3, x_5, x_6 completely determine $\mathcal{R}(\boldsymbol{w})$.

3. Graphical Characterization of Feasible Equilibrium Region

The k-contact feasible equilibrium region is the convex hull of the pairwise feasible equilibrium strips (Proposition 1). Hence we focus on the graphical characterization of the individual 2-contact equilibrium strips, with the understanding that the convex hull of the pairwise strips is a strip bounded by their leftmost and rightmost edges.

First consider the 2-contact equilibrium strip associated with the nominal gravitational wrench $\boldsymbol{w}_0 = (f_g, 0)$. In this case $\mathcal{R}(\boldsymbol{w}_0)$ is a vertical strip that can be obtained by union and intersection of *five* strips, each having a distinct geometric interpretation. The five strips are as follows. Let $\mathcal{C}_i^-$ denote the negative reflection of the friction cone $\mathcal{C}_i$ about its base point x_i. Let S_0^{++} denote the infinite vertical strip spanned by the polygon $\mathcal{C}_1 \cap \mathcal{C}_2$. Similarly, let S_0^{+-}, S_0^{-+}, and S_0^{--} denote the infinite vertical strips spanned by the polygons $\mathcal{C}_1^+ \cap \mathcal{C}_2^-$, $\mathcal{C}_1^- \cap \mathcal{C}_2^+$, and $\mathcal{C}_1^- \cap \mathcal{C}_2^-$. Note that some of these polygons and their associated strips may be empty. The fifth strip, denoted Π_0, is the infinite vertical strip bounded by the contacts x_1 and x_2. The graphical construction of $\mathcal{R}(\boldsymbol{w}_0)$ is summarized in the following lemma.

LEMMA 1. Let $\mathcal{B}$ be supported by two frictional contacts in a two-dimensional gravitational environment, and be subjected to a nominal gravitational wrench $\boldsymbol{w}_0 = (f_g, 0)$. Then the feasible equilibrium region $\mathcal{R}(\boldsymbol{w}_0)$ is an infinite vertical strip given by

$$\mathcal{R}(\boldsymbol{w}_0) = \left((S_0^{++} \cup S_0^{--}) \cap \Pi_0\right) \cup \left((S_0^{+-} \cup S_0^{-+}) \cap \bar{\Pi}_0\right), \quad (4)$$

where $\bar{\Pi}_0$ is the complement of Π_0 in $I\!R^2$.

Proof. There are three external forces acting on $\mathcal{B}$: the gravitational force f_g acing at x, and the contact forces f_1 and f_2 acting at x_1 and x_2. The net moment generated by these forces must vanish at an equilibrium. It can be verified that vanishing of the net moment implies that the three force lines intersect at a common point denoted z (in the special case where all forces are parallel, z lies at infinity). Since each f_i must lie in its friction cone $\mathcal{C}_i$, the point z must lie in the intersection of the double-cones $\mathcal{C}_1 \cup \mathcal{C}_1^-$ and $\mathcal{C}_2 \cup \mathcal{C}_2^-$. The line of f_g passes through both x and z. Hence concurrency of the three force lines implies that x must lie in one of the infinite vertical strips spanned by the intersection $(\mathcal{C}_1 \cup \mathcal{C}_1^-) \cap (\mathcal{C}_2 \cup \mathcal{C}_2^-)$. These are precisely the four strips S_0^{++}, S_0^{+-}, S_0^{-+}, and S_0^{--} (Figure 3(a)-(b)).

Next consider the force equation $f_1 + f_2 + f_g = 0$. Note that even though the concurrency point z can lie in the double-cone $\mathcal{C}_i \cup \mathcal{C}_i^-$, the contact force f_i can lie only in the positive cone $\mathcal{C}_i$ for $i = 1, 2$. Let u_i be a unit vector from x_i to z $(i = 1, 2)$. There are four cases to consider depending on the location of the concurrency point z. First consider the case where $z \in \mathcal{C}_1 \cap \mathcal{C}_2$. In this case $u_1 \in \mathcal{C}_1$ and $u_2 \in \mathcal{C}_2$. Hence each f_i can be written as $f_i = \alpha_i u_i$ for some $\alpha_i \geq 0$. Let $f_g^\perp = J f_g$ denote the horizontal direction. Multiplying the equation $f_1 + f_2 + f_g = 0$ by $f_g^\perp$ gives: $\alpha_1(u_1 \cdot f_g^\perp) + \alpha_2(u_2 \cdot f_g^\perp) = 0$. Since $\alpha_i \geq 0$, we conclude that $u_1 \cdot f_g^\perp$ and $u_2 \cdot f_g^\perp$ must have opposite signs. The graphical interpretation of this fact is that z must lie *inside* the vertical strip Π_0 bounded by x_1 and x_2. Since x and z lie on a common vertical line, x must lie in the intersection $S_0^{++} \cap \Pi_0$ (Figure 3(c)). Next consider the case where $z \in \mathcal{C}_1 \cap \mathcal{C}_2^-$. In this case $u_1 \in \mathcal{C}_1$ while $u_2 \in \mathcal{C}_2^-$. Hence $f_i = \alpha_i u_i$ such that $\alpha_1 \geq 0$ and $\alpha_2 \leq 0$. The equation $\alpha_1(u_1 \cdot f_g^\perp) + \alpha_2(u_2 \cdot f_g^\perp) = 0$ now implies that $u_1 \cdot f_g^\perp$ and $u_2 \cdot f_g^\perp$ must have the same sign. The graphical interpretation of this fact is that z must lie *outside* the vertical strip Π_0. Thus, x lies in the intersection $S_0^{+-} \cap \bar{\Pi}_0$. By applying similar

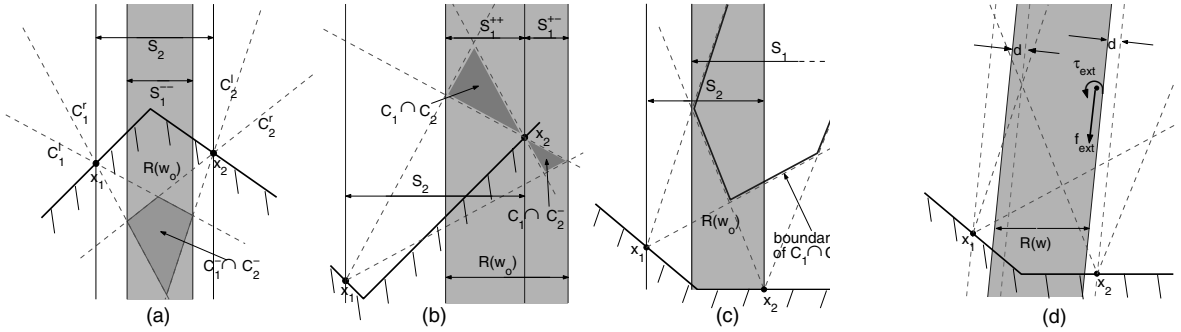

Fig. 3. Graphical characterization of $\mathcal{R}(\boldsymbol{w})$ in four cases: (a) $\mathcal{R}(\boldsymbol{w}_0) = S^{--} \cap \Pi$, (b) $\mathcal{R}(\boldsymbol{w}_0) = S^{++} \cup S^{+-}$, (c) $\mathcal{R}(\boldsymbol{w}_0) = S_1^{++} \cap \Pi$, (d) $\mathcal{R}(\boldsymbol{w})$ for a general wrench $\boldsymbol{w} = (f_{ext}, \tau_{ext})$.

arguments to the remaining two cases where $z \in \mathcal{C}_1^- \cap \mathcal{C}_2^-$ and $z \in \mathcal{C}_1^- \cap \mathcal{C}_2$, formula (4) is obtained. □

Note that the five vertical strips comprising $\mathcal{R}(\boldsymbol{w}_0)$ always form a *single connected strip* (Theorem 1). The graphical characterization of $\mathcal{R}(\boldsymbol{w}_0)$ also captures the situations where $\mathcal{R}(\boldsymbol{w}_0)$ is unbounded, as in the example of Figure 2(b). The graphical characterization is consistent with the analysis provided in Bret et al. (2003) for three-legged climbing, and with the characterization given in Erdmann (1998) for object manipulation under the influence of gravity. It is also worth discussing the *moment labelling* technique developed for pushing applications in planar environments. This technique depicts the net reaction wrench generated by k frictional contacts in terms of signed polygons P_- and P_+. All lines passing between the two polygons in a direction determined by their sign are possible reaction wrenches. In particular, $\mathcal{R}(\boldsymbol{w}_0)$ is the vertical strip bounded by P_- and P_+. Moment labelling can thus provide an alternative to our graphical technique of taking the convex hull of pairwise strips.

EXAMPLE 3. Consider formula (4) for the special case where the two contacts lie on a common terrain segment. If the two friction cones contain the upward vertical direction, $S_0^{++} = S_0^{--} = \mathbb{R}^2$ and $S_0^{+-} = S_0^{-+} = \emptyset$. In this case $\mathcal{R}(\boldsymbol{w}_0) = \Pi_0$. This special case still holds true when the two contacts lie on disjoint pieces of the line segment joining the contacts.

Consider now the graphical characterization of the 2-contact feasible equilibrium strip for a general external wrench $\boldsymbol{w} = (f_{ext}, \tau_{ext})$. When $\tau_{ext} = 0$ the net force $f_{ext} = f_g + f_d$ acts along a line passing through the center of mass of $\mathcal{B}$, but now the line is rotated with respect to the vertical direction. In this case the feasible equilibrium region is constructed by the same procedure described above, except that now the five vertical strips are rotated to match the direction of f_{ext}. When $\tau_{ext} \neq 0$, the wrench $\boldsymbol{w}$ is equivalent to a pure force f_{ext} acting on $\mathcal{B}$ along a line having a perpendicular offset d from x, where $d = \tau_{ext}/\|f_{ext}\|$. Hence the five strips are rotated and parallel shifted by $-d$ as shown in Figure 3(d). The following lemma summarizes the construction of the general 2-contact feasible equilibrium strip.

LEMMA 2. Let $\mathcal{B}$ be supported by two frictional contacts in a two-dimensional gravitational environment, and be subjected a net external wrench $\boldsymbol{w} = (f_{ext}, \tau_{ext})$. Let S^{++}, S^{+-}, S^{-+}, S^{--} be the strips spanned by the polygons $\mathcal{C}_1 \cap \mathcal{C}_2$, $\mathcal{C}_1^+ \cap \mathcal{C}_2^-$, $\mathcal{C}_1^- \cap \mathcal{C}_2^+$, $\mathcal{C}_1^- \cap \mathcal{C}_2^-$, and let Π be the strip bounded by x_1 and x_2, such that the five strips are parallel to f_{ext} and parallel shifted by $-\tau_{ext}/\|f_{ext}\|$. Then the feasible equilibrium region $\mathcal{R}(\boldsymbol{w})$ is an infinite strip parallel to f_{ext} given by

$$\mathcal{R}(\boldsymbol{w}) = \left((S^{++} \cup S^{--}) \cap \Pi\right) \cup \left((S^{+-} \cup S^{-+}) \cap \bar{\Pi}\right),$$

where $\bar{\Pi}$ is the complement of Π in $\mathbb{R}^2$.

Line sweep algorithm for computing $\mathcal{R}(\boldsymbol{w})$. The feasible equilibrium strip of a k-contact stance can be computed as the convex hull of all pairwise strips in $O(k^2)$ steps. We describe in Appendix B a more sophisticated line-sweep algorithm that computes $\mathcal{R}(\boldsymbol{w})$ in practically $O(k)$ steps. The main steps of the algorithm for the case of $\boldsymbol{w}_0 = (f_g, 0)$ are as follows. The algorithm stores the $2k$ directed lines aligned with the edges of the friction cones in lists $\mathcal{L}_1$ and $\mathcal{L}_2$. The list $\mathcal{L}_1$ contains the lines pointing to the *left* of the upward vertical direction, while $\mathcal{L}_2$ contains the lines pointing to the *right* of the upward vertical direction. The set of intersection points of left-pointing lines with right-pointing lines is denoted $\mathcal{S}$. A key fact is that the edges of $\mathcal{R}(\boldsymbol{w}_0)$ are vertical lines passing through the leftmost and rightmost points of $\mathcal{S}$. Let us next consider the computation of the right edge of $\mathcal{R}(\boldsymbol{w}_0)$ or, equivalently, the rightmost point of $\mathcal{S}$. The algorithm computes in $O(k)$ steps a line $l'(0)$ on the right side of $\mathcal{S}$. The algorithm also selects a suitable initial point of $\mathcal{S}$, and defines the vertical line through this point as the initial sweep line $l(0)$. At the i^{th} iteration the algorithm selects a vertical line at the middle of the strip bounded by $l(i)$ and $l'(i)$. Then it checks whether

the middle line lies to the right of $\mathcal{S}$. If it does, the middle line becomes $l'(i+1)$ and $l(i+1)$ moves to a new point of $\mathcal{S}$ on the right side of $l(i)$. Otherwise $l'(i+1) = l'(i)$, and $l(i+1)$ moves to a point of $\mathcal{S}$ which lies on the right side of the middle line. The algorithm next inspects the intersection pattern of the lines of $\mathcal{L}_1$ and $\mathcal{L}_2$ with $l(i+1)$, and removes from these lists lines that do not affect the points of $\mathcal{S}$ on the right side of $l(i+1)$. The iterations repeat until $\mathcal{L}_1$ and $\mathcal{L}_2$ become simultaneously empty. At this stage $l(i+1)$ has reached the rightmost point of $\mathcal{S}$ and the algorithm terminates.

The computational complexity of the algorithm is as follows. As discussed in the appendix, at least one line is removed from $\mathcal{L}_1$ or $\mathcal{L}_2$ in each iteration. Hence there are $O(k)$ iterations. The number of iterations is also bounded by the binary bisection to $\log(\Delta/\delta)$, where Δ is the initial search width and δ is the minimal search width. Since each iteration takes $O(k)$ steps, the total run-time is $k \cdot \min\{k, \log(\Delta/\delta)\}$. In practical settings $\log(\Delta/\delta)$ is a small constant, and the algorithm runs in $O(k)$ steps. An execution example of the algorithm on a 6-contact stance is provided in the appendix.

4. The Robust Equilibrium Region

So far we have focused on the feasible equilibrium region of a k-contact stance associated with a specific external wrench. In this section we consider the robust equilibrium region associated with neighborhoods of external wrenches. The wrench neighborhoods represent inertial forces generated by moving limbs of the mechanism, but can also represent environmental disturbances as well as positioning inaccuracies. First we introduce a convenient parameterization for wrench neighborhoods and define the robust equilibrium region. Then we formulate the computation of the robust equilibrium region as a linear programming problem, and finally discuss its graphical construction.

4.1. Parametrization of the Wrench Neighborhood $\mathcal{W}$

The wrench parametrization is based on the following homogeneity property. If $\boldsymbol{f}$ is the $2k$-vector of reaction forces satisfying the equilibrium condition (1) for $\boldsymbol{w}_{ext}$, then $s\boldsymbol{f}$ satisfies (1) for $s\boldsymbol{w}_{ext}$ where s is a positive scalar. Let (f_x, f_y) denote the horizontal and vertical coordinates of f_{ext}. Since $f_{ext} = f_g + f_d$ such that f_g is vertical and $\|f_d\| \ll \|f_g\|$, we may assume that $f_y \neq 0$. Thus we define *homogeneous coordinates* for wrench space as (p, q), where $p \triangleq f_x/f_y$ and $q \triangleq \tau_{ext}/f_y$. The (p, q) coordinates can be interpreted as follows. The nominal gravitational wrench, $\boldsymbol{w}_o = (f_g, 0)$, corresponds to $(p, q) = (0, 0)$. Any other wrench $\boldsymbol{w} = (f_{ext}, \tau_{ext}) \in \mathbb{R}^2 \times \mathbb{R}$ can be represented by its magnitude and an oriented line of action. The wrench's line of action is oriented along f_{ext}, and the horizontal distance of this line from $\mathcal{B}$'s center-of-mass is τ_{ext}/f_y. Hence p represents the orientation of the wrench's line of action, and q represents its horizontal distance from $\mathcal{B}$'s center of mass at x. Using (p, q), we assume that $\mathcal{W}$ is a *rectangular neighborhood* given by $\mathcal{W} = \{(p, q) : \kappa_1 \leq p \leq \kappa_2, \nu_1 \leq q \leq \nu_2\}$, where κ_i and ν_i are given constants for $i = 1, 2$. Note that $\mathcal{W}$ is specified relative to the gravitational wrench in a way that is independent of the choice of world and body frames. The definition of the robust equilibrium region associated with $\mathcal{W}$ is as follows.

DEFINITION 2. Given a k-contact stance and a neighborhood $\mathcal{W}$ of external wrenches acting on $\mathcal{B}$, the **robust equilibrium region** of $\mathcal{W}$, denoted $\mathcal{R}(\mathcal{W})$, is the set of $\mathcal{B}$'s center-of-mass locations at which all wrenches of $\mathcal{W}$ possess feasible contact forces $f_i \in \mathcal{C}_i$ $(i = 1 \ldots k)$ satisfying the equilibrium equation (1).

The robust equilibrium region can be equivalently defined as the intersection of the feasible equilibrium strips associated with the individual wrenches in $\mathcal{W}$ i.e., $\mathcal{R}(\mathcal{W}) = \cap_{\boldsymbol{w} \in \mathcal{W}} \mathcal{R}(\boldsymbol{w})$.

4.2. Computation of the Robust Equilibrium Region

We now show how to compute the robust equilibrium region as a linear programming problem. In order to obtain the (p, q) version of the equilibrium condition (1), we divide both sides of (1) by $f_y \neq 0$ and obtain the equivalent equilibrium condition:

$$\begin{bmatrix} G_f \\ G_\tau \end{bmatrix} \boldsymbol{f} = -\begin{pmatrix} p \\ 1 \\ \tau(x) \end{pmatrix}, \tag{5}$$

where $\boldsymbol{f} \geq \vec{0}$ and $\tau(x) = x^T J^T \begin{pmatrix} p \\ 1 \end{pmatrix} + q$. The following theorem characterizes the robust equilibrium region as a linear programming problem.

THEOREM 2. Let $\mathcal{B}$ be supported by k frictional contacts in a two-dimensional gravitational environment, and be subjected to a neighborhood $\mathcal{W} = [\kappa_1, \kappa_2] \times [\nu_1, \nu_2]$ of disturbance wrenches. Then the robust equilibrium region of $\mathcal{W}$ is a **finite parallelogram** given by

$$\mathcal{R}(\mathcal{W}) = \Big\{ x \in \mathbb{R}^2 : \tau_{1,min} - \nu_1 \leq x^T J^T f^1_{ext} \leq \tau_{1,max} - \nu_2 \quad \text{and} \quad \tau_{2,min} - \nu_1 \leq x^T J^T f^2_{ext} \leq \tau_{2,max} - \nu_2 \Big\},$$

where $f^i_{ext} = (\kappa_i, 1)$ for $i = 1, 2$, and $\tau_{i,min}$, $\tau_{i,max}$ are obtained by solving the linear programming problems:

$$\begin{aligned} \tau_{i,min} &= \min_{G_f \boldsymbol{f} = -f^i_{ext},\, \boldsymbol{f} \geq \vec{0}} \{-G_\tau \boldsymbol{f}\} \\ \tau_{i,max} &= \max_{G_f \boldsymbol{f} = -f^i_{ext},\, \boldsymbol{f} \geq \vec{0}} \{-G_\tau \boldsymbol{f}\} \end{aligned} \quad \text{for } i = 1, 2. \tag{6}$$

Proof. The wrenches parametrized by the vertices of $\mathcal{W} = [\kappa_1, \kappa_2] \times [\nu_1, \nu_2]$ are: $\boldsymbol{w}_{11} = (f^1_{ext}, \nu_1)$, $\boldsymbol{w}_{12} = (f^1_{ext}, \nu_2)$, $\boldsymbol{w}_{21} = (f^2_{ext}, \nu_1)$, $\boldsymbol{w}_{22} = (f^2_{ext}, \nu_2)$, where $f^i_{ext} = (\kappa_i, 1)$ for

$i = 1, 2$. Let $\widetilde{\mathcal{R}}(\mathcal{W})$ be the intersection of the feasible equilibrium strips associated with these four wrenches. We first show that $\widetilde{\mathcal{R}}(\mathcal{W})$ is the parallelogram of the theorem, then show that $\mathcal{R}(\mathcal{W}) = \widetilde{\mathcal{R}}(\mathcal{W})$. Using Theorem 1 with $\tau_{i,min}$ and $\tau_{i,max}$, the strips $\mathcal{R}(\boldsymbol{w}_{ij})$ are given by $\mathcal{R}(\boldsymbol{w}_{ij}) = \{x : \tau_{i,min} - \nu_j \leq x^T J f^i_{ext} \leq \tau_{i,max} - \nu_j\}$ for $1 \leq i, j \leq 2$. Since ν_j appears as a linear additive term in $\mathcal{R}(\boldsymbol{w}_{ij})$ and $\nu_1 \leq \nu_2$, the intersection $\widetilde{\mathcal{R}}(\mathcal{W})$ can be written as

$$\widetilde{\mathcal{R}}(\mathcal{W}) = \{x \in I\!R^2 : \tau_{i,min} - \nu_1 \leq x^T J f^i_{ext} \leq \tau_{i,max} - \nu_2 \quad \text{for } i = 1, 2\},$$

which is the parallelogram specified in the theorem. Next we prove that $\mathcal{R}(\mathcal{W}) = \widetilde{\mathcal{R}}(\mathcal{W})$ in two steps. First we show that $\mathcal{R}(\mathcal{W}) \subseteq \widetilde{\mathcal{R}}(\mathcal{W})$, then we show that $\widetilde{\mathcal{R}}(\mathcal{W}) \subseteq \mathcal{R}(\mathcal{W})$.

1. Let $x \in \mathcal{R}(\mathcal{W})$. Then by definition x lies in $\mathcal{R}(\boldsymbol{w})$ for all $\boldsymbol{w} \in \mathcal{W}$. In particular, x lies in $\mathcal{R}(\boldsymbol{w}_{ij})$ for $1 \leq i, j \leq 2$, which implies that $x \in \widetilde{\mathcal{R}}(\mathcal{W})$.

2. Let $x \in \widetilde{\mathcal{R}}(\mathcal{W})$. Then by definition x lies in $\mathcal{R}(\boldsymbol{w}_{ij})$ for $1 \leq i, j \leq 2$. Hence there exist $2k$-vectors $\boldsymbol{f}_{ij} \geq \vec{0}$ satisfying the equilibrium condition

$$\begin{aligned} G_f \boldsymbol{f}_{ij} &= -f^i_{ext} \\ G_\tau \boldsymbol{f}_{ij} &= -(x^T J^T f^i_{ext} + \nu_j) \end{aligned} \qquad \text{for } 1 \leq i, j \leq 2. \tag{7}$$

We now show that x lies in the individual strips $\mathcal{R}(\boldsymbol{w})$ for all $\boldsymbol{w}$ parametrized by $\mathcal{W}$. Any (p, q) in $\mathcal{W} = [\kappa_1, \kappa_2] \times [\nu_1, \nu_2]$ can be expressed as a convex combination of the four vertices:

$$\begin{pmatrix} p \\ q \end{pmatrix} = \lambda_{11} \begin{pmatrix} \kappa_1 \\ \nu_1 \end{pmatrix} + \lambda_{12} \begin{pmatrix} \kappa_1 \\ \nu_2 \end{pmatrix} + \lambda_{21} \begin{pmatrix} \kappa_2 \\ \nu_1 \end{pmatrix} + \lambda_{22} \begin{pmatrix} \kappa_2 \\ \nu_2 \end{pmatrix},$$

where $\lambda_{ij} \in [0, 1]$ and $\sum_{i,j} \lambda_{ij} = 1$ for $1 \leq i, j \leq 2$. Writing $\boldsymbol{w} = (f_{ext}, \tau_{ext})$ such that $f_{ext} = (p, 1)$ and $\tau_{ext} = q$, we have that $f_{ext} = (\lambda_{11} + \lambda_{12}) f^1_{ext} + (\lambda_{21} + \lambda_{22}) f^2_{ext}$ and $\tau_{ext} = (\lambda_{11} + \lambda_{21})\nu_1 + (\lambda_{21} + \lambda_{22})\nu_2$. It follows that the vector of contact forces $\boldsymbol{f} = \sum_{i,j} \lambda_{ij} \boldsymbol{f}_{ij} \geq \vec{0}$ satisfies

$$\begin{aligned} G_f \boldsymbol{f} &= \sum_{i,j} \lambda_{ij} G_f \boldsymbol{f}_{ij} = -(\lambda_{11} + \lambda_{12}) f^1_{ext} \\ &\quad - (\lambda_{21} + \lambda_{22}) f^2_{ext} = -f_{ext} \\ G_\tau \boldsymbol{f} &= \sum_{i,j} \lambda_{ij} G_\tau \boldsymbol{f}_{ij} = -x^T J^T \big((\lambda_{11} + \lambda_{12}) f^1_{ext} \\ &\quad + (\lambda_{21} + \lambda_{22}) f^2_{ext}\big) - \big((\lambda_{11} + \lambda_{21})\nu_1 \\ &\quad + (\lambda_{21} + \lambda_{22})\nu_2\big) = -(x^T J^T f_{ext} + \tau_{ext}). \end{aligned}$$

Thus $\boldsymbol{f}$ satisfies the equilibrium condition (5) for $\boldsymbol{w} = (f_{ext}, \tau_{ext})$ and center of mass at x. Hence $x \in \mathcal{R}(\boldsymbol{w})$. Since the above argument holds for all $\boldsymbol{w}$ parametrized by $\mathcal{W}$, we conclude that $x \in \mathcal{R}(\mathcal{W})$. □

The theorem can easily be extended to wrench neighborhoods $\mathcal{W}$ specified as convex polygons in the (p, q) plane. In this case $\mathcal{R}(\mathcal{W})$ is the intersection of the feasible equilibrium strips associated with the external wrenches parametrized by the vertices of $\mathcal{W}$. The theorem specifies a graphical construction of $\mathcal{R}(\mathcal{W})$ as a parallelogram obtained by intersecting the feasible equilibrium strips associated with the vertices of $\mathcal{W}$. This construction is illustrated in the following example.

EXAMPLE 4. Consider the 2-contact stance shown in Figure 4(b), where the coefficient of friction is $\mu = 0.4$. We selected a rectangular wrench neighborhood $\mathcal{W} = [-\kappa, \kappa] \times [-\nu, \nu]$ with $\kappa = 0.3$ and $\nu = \|x_2 - x_1\|/8$. The neighborhood $\mathcal{W}$ is depicted in Figure 4(a) as a sector of force-directions representing the interval $[-\kappa, \kappa]$, and a strip of force-lines representing the interval $[-\nu, \nu]$. Figure 4(b) shows the strips $\mathcal{R}(\boldsymbol{w}_{ij})$ associated with the vertices of $\mathcal{W}$, where each strip is constructed graphically using Lemma 2. The robust equilibrium region is the shaded parallelogram obtained by intersecting the four strips.

The example illustrates an important property of the robust equilibrium region. *No matter how small the wrench neighborhood $\mathcal{W}$, it always imposes an upper limit on the height of $\mathcal{B}$'s center-of-mass locations.* In other words, as the height of $\mathcal{B}$'s center of mass above the contacts increases, the neighborhood $\mathcal{W}$ must shrink so that $\mathcal{B}$'s center of mass remains in the robust equilibrium region.

Line sweep algorithm for computing $\mathcal{R}(\mathcal{W})$. In principle one can invoke the line-sweep algorithm of the previous section for each vertex of $\mathcal{W}$, then intersect the resulting strips. But a more efficient use of the line-sweep algorithm is as follows. The neighborhood $\mathcal{W} = [-\kappa, \kappa] \times [-\nu, \nu]$ crosses the p-axis at $(\kappa_1, 0)$ and $(\kappa_2, 0)$. These points represent zero-torque wrenches with f_{ext} at the extreme orientations κ_1 and κ_2. By invoking the line-sweep algorithm at these two points rather than at the four vertices, one obtains two feasible equilibrium strips that can be processed as follows. The bounding lines of the two strips are parallel shifted by $-\tau_{ext}/\|f_{ext}\|$, using the values (f_{ext}, τ_{ext}) at the vertices of $\mathcal{W}$. This gives two narrower strips, and their intersection is precisely $\mathcal{R}(\mathcal{W})$.

5. Experimental Results

We describe preliminary experiments that measure the static response of a two-legged prototype to disturbance forces. The goal of these experiments is to validate the stance equilibrium criteria for an object supported by frictional contacts against gravity and subjected to disturbance forces. The experimental

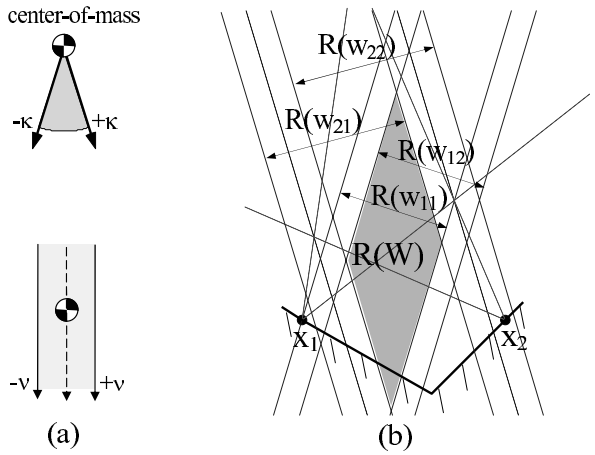

Fig. 4. (a) Depiction of the wrench neighborhood $\mathcal{W} = [-\kappa, \kappa] \times [-\nu, \nu]$. (b) The robust equilibrium region is the parallelogram $\mathcal{R}(\mathcal{W})$.

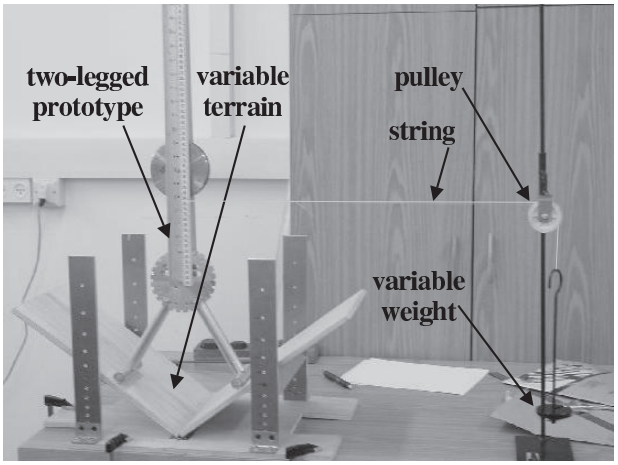

Fig. 5. Experimental setup of a two-legged prototype.

system shown in Figure 5 consists of a two-legged prototype made of aluminium. The center-of-mass position can be freely changed by sliding a heavy weight on a bar mounted on a rotational joint. However, the experiments focus on the response to varying disturbance forces with a fixed center-of-mass position. The mechanism is placed on terrain made of two rigid segments with adjustable slopes. The segments in the experiments form a symmetric v-shaped terrain with fixed slopes of $\alpha = 26.7°$. The contacts are placed at equal heights on the two segments, at a horizontal distance $l = 237$ mm from each other. A horizontal force f_d is applied to the mechanism by a variable weight hung on a string attached through a pulley to the mechanism's central bar. The magnitude of f_d is then gradually increased until it reaches a critical value at which the contacts break, roll, or slip. The critical force is recorded, and the process is repeated for different heights of f_d's application point. Note that the measurements span a neighborhood about the origin in the (p, q) parametrization of the previous section: the variation in magnitude of f_d varies the orientation parameter p, and the variation in height of f_d varies the torque parameter q. As a preliminary step, the coefficient of friction was experimentally determined to be $\mu = 0.25$ with a standard deviation of $\pm 6.5\%$.

Let us first analyze the mechanism's response to varying disturbance forces. Let h denote the height of f_d's application point above the contacts. The disturbance force has variable magnitude and application point height. The gravitational force has a constant magnitude mg, where $m = 2.4$ kg and g is the gravity constant. The net external force, $f_{ext} = f_g + f_d$, acts through the string attachment point at an angle $\beta = \tan^{-1}(\|f_d\|/mg)$ with respect to the vertical direction. The contact reaction forces are statically indeterminate in this setup, but critical events where an equilibrium ceases to be feasible can be determined as follows. Consider the case where f_d is directed to the right. In this case two critical events can occur. The first event occurs when the line of f_{ext} passes through x_2 (Figure 6(a)). In this case the contact reaction force at x_1 vanishes, resulting in contact breakage at x_1 and rolling about x_2. The corresponding critical force angle is $\beta_1 = \tan^{-1}(l/2h)$. The second event occurs when the line of f_{ext} passes through the intersection point of the right edges of the friction cones (p_{rr} in Figure 6(b)). In this case both contacts start sliding to the

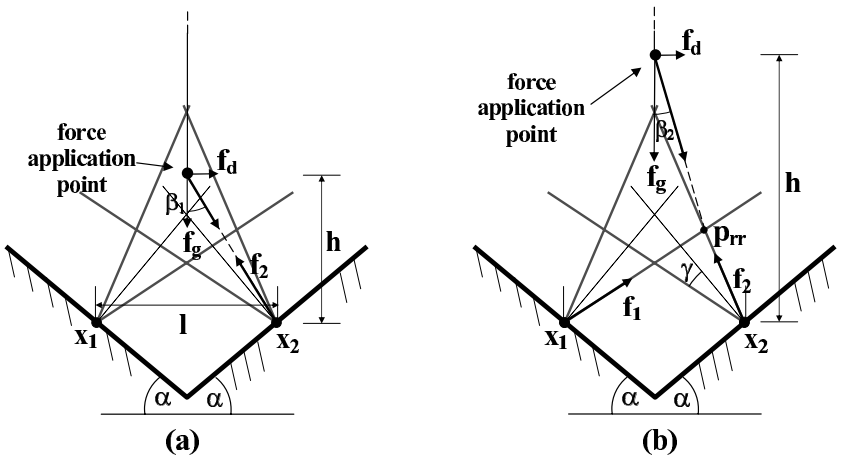

Fig. 6. Graphical characterization of critical disturbance force: (a) $\|f_d\| = mg\tan(\beta_1)$, and (b) $\|f_d\| = mg\tan(\beta_2)$.

left, and the contact reaction forces lie on the right edges of the friction cones. The corresponding critical force angle is $\beta_2 = \tan^{-1}\left(l\sin 2\gamma/(2h\sin 2\gamma - l\cos 2\alpha - l\cos 2\gamma)\right)$, where $\gamma = \tan^{-1}(\mu) = 13.8°$. The critical disturbance force associated with contact breakage or sliding has magnitude $\|f_d\| = mg\tan(\beta)$ where $\beta = \min\{\beta_1, \beta_2\}$. The event dominating $\min\{\beta_1, \beta_2\}$ can be determined as a function of the application point of f_d as follows. When the application point of f_d lies inside the polygon $\mathcal{C}_1 \cap \mathcal{C}_2$ as in Figure 6(a), $\beta_1 < \beta_2$ and the mechanism starts rolling about x_2. When the application point of f_d lies above $\mathcal{C}_1 \cap \mathcal{C}_2$ as in Figure 6(b), $\beta_2 < \beta_1$ and the mechanism starts sliding at both contacts.

The experimental results are presented in Figure 7. For each force application height five experiments were conducted, and the average critical $\|f_d\|$ was measured with its corresponding angle β. In order to present a linear relationship, we plot $\cot(\beta)$ as a function of h. The dashed and solid lines are $\cot(\beta_1)$ and $\cot(\beta_2)$, computed analytically as a function of h. Since $\beta = \min\{\beta_1, \beta_2\}$, the experimental results were expected to follow the line of $\cot(\beta_1)$ for $h < h_0$, then follow the line of $\cot(\beta_2)$ for $h > h_0$. The height h_0 occurs when the application point of f_d lies at the top of the polygon $\mathcal{C}_1 \cap \mathcal{C}_2$, given by $h_0 = l\cot(\alpha-\gamma)/2 = 517$ mm. The experimental results are marked as dots with error bars of two standard deviations. One can see close matching of the predicted behavior with the experimental results. The close matching validates the criteria employed in the construction of the robust equilibrium region. The experiments also indicate that feasible equilibrium stances are generated by the mechanism without any dynamic ambiguity. This topic is further discussed in Or and Rimon (2004).

More extensive experiments with a 3-legged robot are currently under preparation (see Figure 1). In these experiments the robot either supports itself on three legs while adjusting its center-of-mass position, or it supports itself on two legs while lifting a third leg to a new position. Both phases involve inertial forces generated by moving parts of the mechanism. These forces act as disturbances on the contacts, and the experiments will verify that selection of robust postures allows the contacts to passively resist these disturbance forces.

6. 3D Frictional Equilibrium Stances

The notion of posture robustness generalizes to three dimensions, but its actual computation is a challenging problem. The most basic component of posture robustness is the feasible equilibrium region associated with the nominal gravitational wrench, denoted $\mathcal{R}_{3D}(\boldsymbol{w}_0)$. This section focuses on basic properties of $\mathcal{R}_{3D}(\boldsymbol{w}_0)$ and the issues involved in its future computation. Thus $\mathcal{B}$ is now a solid object supported by k frictional contacts in a three-dimensional gravitational environment. The equilibrium condition associated with the gravitational wrench $\boldsymbol{w}_0 = (f_g, 0) \in I\!R^6$ is:

$$\sum_{i=1}^{k} \begin{pmatrix} f_i \\ x_i \times f_i \end{pmatrix} = -\begin{pmatrix} f_g \\ x \times f_g \end{pmatrix}, \tag{8}$$

where x_i is the i^{th} contact, x is the position of $\mathcal{B}$'s center-of-mass, f_i is the i^{th} contact reaction force, and f_g is the gravitational force acting at x. The contact forces must additionally lie in their respective friction cones which are defined as follows. Let n_i be the outward unit normal at x_i, and let s_i, t_i be unit tangents at x_i such that (s_i, t_i, n_i) is a right-handed frame. Then $\mathcal{C}_i = \{f_i : f_i \cdot n_i \geq 0,\ (f_i \cdot s_i)^2 + (f_i \cdot t_i)^2 \leq (\mu f_i \cdot n_i)^2\}$ where μ is the coefficient of friction. Note that $\mathcal{C}_i$ is now defined in terms of linear as well as quadratic inequalities. As discussed below, an exact computation of $\mathcal{R}_{3D}(\boldsymbol{w}_0)$ based on

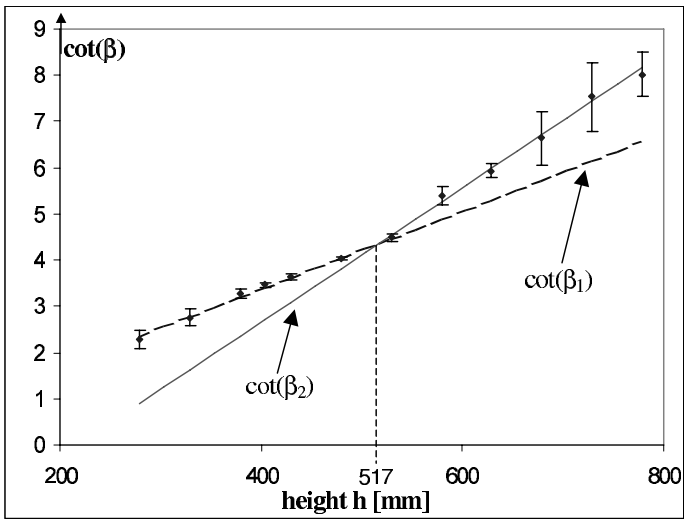

Fig. 7. Experimental (dots) and theoretical (solid and dashed lines) results of $\cot(\beta)$ as a function of h. The bars represent two standard deviations.

the quadratic friction cones results in a semi-algebraic system of polynomials.

The definition of $\mathcal{R}_{3D}(\boldsymbol{w}_0)$ is as follows. For a given k-contact stance, the *feasible equilibrium region* associated with $\boldsymbol{w}_0$ consists of all $\mathcal{B}$'s center-of-mass locations for which there exist contact reaction forces $f_i \in \mathcal{C}_i$ for $i = 1 \ldots k$ satisfying the equilibrium equation (8). The following proposition summarizes some basic properties of this region.

PROPOSITION 2. Let a solid object $\mathcal{B}$ be supported by k frictional contacts against gravity in three dimensions. If the feasible equilibrium region $\mathcal{R}_{3D}(\boldsymbol{w}_0)$ is nonempty, it is generically a vertical line for a single contact, a vertical strip for two contacts, and a three-dimensional **vertical convex prism** for $k \geq 3$ contacts.

For a single contact $\mathcal{R}_{3D}(\boldsymbol{w}_0)$ is a vertical line through the contact, and for two contacts it is a vertical strip in the plane passing through the contacts. For $k \geq 3$ contacts $\mathcal{R}_{3D}(\boldsymbol{w}_0)$ is a vertical prism whose position has no obvious relation to the position of the contacts. However, $\mathcal{R}_{3D}(\boldsymbol{w}_0)$ contains the contacts in the special case where all friction cones contain the upward vertical direction. This special case is related to the familiar support polygon principle discussed below.

Proof. We first verify that $\mathcal{R}_{3D}(\boldsymbol{w}_0)$ consists of entire vertical lines. Let e denote the upward vertical direction, and let x be a point in $\mathcal{R}_{3D}(\boldsymbol{w}_0)$. Since f_g is vertical, the right side of (8) satisfies $(x + se) \times f_g = x \times f_g$ for all $s \in \mathbb{R}$. Hence the entire vertical line $\{x + se,\ s \in \mathbb{R}\}$ is contained in $\mathcal{R}_{3D}(\boldsymbol{w}_0)$, which therefore consists of entire vertical lines. Next we show that $\mathcal{R}_{3D}(\boldsymbol{w}_0)$ is connected and convex. Let x' and x'' be two points in $\mathcal{R}_{3D}(\boldsymbol{w}_0)$, and let f_i', $f_i'' \in \mathcal{C}_i$ $(i = 1 \ldots k)$ be the contact forces satisfying (8) for x' and x''. Any point on the line segment joining x' and x'' can be written as $x(\lambda) = \lambda x' + (1-\lambda)x''$ for some $\lambda \in [0, 1]$. The corresponding contact forces $f_i = \lambda f_i' + (1 - \lambda) f_i''$ lie in $\mathcal{C}_i$ and satisfy the equilibrium equation (8) with $x = x(\lambda)$. Hence $\mathcal{R}_{3D}(\boldsymbol{w}_0)$ is connected as well as convex.

We have established that $\mathcal{R}_{3D}(\boldsymbol{w}_0)$ is a convex prism in physical space $\mathbb{R}^3$. It is left to show that the prism is three-dimensional for $k \geq 3$ contacts (the cases of one and two contacts can be determined by inspection). Let *wrench space* have force-and-torque coordinates $(f, \tau) \in \mathbb{R}^6$. As $\mathcal{B}$'s center of mass varies in physical space, the gravitational wrench on the right side of (8) spans a two-dimensional affine subspace in wrench space (the vertical component of x is mapped to zero). Let L denote this subspace. On the other hand, as the contact forces vary in their friction cones, their net reaction wrench on the left side of (8) spans a cone in wrench space. Let N denote this cone. In order to determine the dimension of the intersection $L \cap N$ we need the following fact. Let $\mathcal{M}$ and $\mathcal{N}$ be m-dimensional and n-dimensional manifolds in $\mathbb{R}^p$. The manifolds meet transversally when the tangent spaces $T_w\mathcal{M}$ and $T_w\mathcal{N}$ span the ambient tangent space $T_w\mathbb{R}^p$ at all points $w \in \mathcal{M} \cap \mathcal{N}$. Transversal intersection of manifolds is generic, and in this case $\mathcal{M} \cap \mathcal{N}$ is a manifold of dimension $m + n - p$ in $\mathbb{R}^p$.

In order to apply the intersection formula, we need to establish the dimension of N and identify under what conditions N and L meet transversally in wrench space. For $k \geq 3$

contacts, a sufficient condition for N to be a six-dimensional cone is that the contacts are not all aligned along some spatial line. A sufficient condition for N and L to meet transversally in wrench space is that the gravitational wrench can be balanced with at least three reaction forces which lie strictly in the interior of their friction cones. Under these generic conditions $N \cap L$ is a two-dimensional planar region in wrench space, since $m+n-p = 6+2-6 = 2$. Finally, the torque generated by f_g is related to the horizontal coordinates of x via the linear mapping $\tau = x \times f_g$. Hence the projection of $N \cap L$ onto the τ-coordinates determines the horizontal cross-section of $\mathcal{R}_{3D}(\boldsymbol{w}_0)$. Since each point of the cross-section determines one vertical line of $\mathcal{R}_{3D}(\boldsymbol{w}_0)$, we conclude that $\mathcal{R}_{3D}(\boldsymbol{w}_0)$ is a three-dimensional prism. □

The Support Polygon Principle. The support polygon principle, known as the tripod rule in three-legged cases, appears in the quasistatic locomotion literature as a posture stability criterion over flat horizontal terrains (Mcghee and Frank 1968). The principle states that $\mathcal{B}$'s center-of-mass must lie in a vertical prism whose cross-section is the convex hull of the contacts. The support polygon provides a simple conservative estimate for $\mathcal{R}_{3D}(\boldsymbol{w}_0)$ over horizontal terrains. It can be verified that it also provides a conservative estimate for $\mathcal{R}_{3D}(\boldsymbol{w}_0)$ on *nearly flat* terrains, defined as terrains in which the upward direction e is contained in all friction cones. However, the support polygon is no longer contained in $\mathcal{R}_{3D}(\boldsymbol{w}_0)$ on general terrains, and in fact may erroneously indicate *unstable* center-of-mass locations. An important challenge is to formulate a practical estimate for $\mathcal{R}_{3D}(\boldsymbol{w}_0)$ that will resemble the classical principle, but would yield only correct stability predictions.

We conclude with a sketch of the issues involved in computing $\mathcal{R}_{3D}(\boldsymbol{w}_0)$ for the basic case of 3-contact stances (Or and Rimon 2006). The contact reaction force f_1, f_2, f_3 are now 3-vectors. Following the reasoning of Theorem 1, the equilibrium and friction constraints take place in the space $(f_1, f_2, f_3, \tau) \cong \mathbb{R}^{12}$ of contact forces and net torque acting on $\mathcal{B}$. These constraints determine a convex set $\mathcal{Q}$ in (f_1, f_2, f_3, τ)-space. Let τ be written as $\tau = (\bar{\tau}, \tau_z)$, where $\bar{\tau} \in \mathbb{R}^2$ is torque about the horizontal axes and τ_z is torque about the vertical axis of a fixed world frame. Then the projection of $\mathcal{Q}$ on the $\bar{\tau}$-coordinates is a convex set in the $\bar{\tau}$-plane. This two-dimensional set is analogous to the interval $[\tau_{min}, \tau_{max}]$ in Theorem 1. The $\bar{\tau}$-projection of $\mathcal{Q}$ determines the horizontal cross section of $\mathcal{R}_{3D}(\boldsymbol{w}_0)$ via the pre-image of the linear mapping $\tau = x \times f_g$. Unfortunately, exact computation of the projection is a major computational challenge. Now $\mathcal{Q}$ is bounded by linear as well as quadratic inequalities. The projection of $\mathcal{Q}$ requires computation of silhouette curves along its boundary which possess total degree 24 in $\mathbb{R}^{12}$ (Or and Rimon 2006). The projection of the latter curves yields algebraic curves of total degree 24 in the $\bar{\tau}$-plane (Or and Rimon 2006). Finally, one has to sort the resulting planar curves in order to determine the region corresponding to the cross-section of $\mathcal{R}_{3D}(\boldsymbol{w}_0)$. An alternative approach is to approximate the $3D$ friction cones by polyhedral cones. In this case $\mathcal{Q}$ becomes a six-dimensional polytope in $\mathbb{R}^{12}$, and the problem becomes the projection of a convex polytope in $\mathbb{R}^{12}$ on the $\bar{\tau}$-plane. Both approaches have a role in future planners. The approximate approach seems to provide efficient computation; the exact approach promises insight and prediction of the situations under which equilibrium can be lost over general terrains.

7. Concluding Discussion

The paper introduced a notion of posture robustness useful for planning quasistatic locomotion over uneven frictional terrains. Focusing on two-dimensional gravitational environments, we lumped the mechanism into a body $\mathcal{B}$ having the same contacts with the environment and a variable center of mass. The wrench neighborhood acting on $\mathcal{B}$ was parametrized as a product of force-direction and force-displacement intervals centered on the gravitational wrench. We showed that the robust equilibrium region of this neighborhoods is a parallelogram that can be computed by linear programs. The parallelogram was also constructed as an intersection of the feasible equilibrium strips associated with the vertices of the wrench neighborhood. An important insight gained from this construction is that posture robustness imposes an *upper limit* on the height of $\mathcal{B}$'s center of mass. Hence when a mechanism executing quasistatic locomotion raises its center of mass, it must accordingly reduce the disturbances generated by its moving limbs in order to maintain posture robustness. This important insight emerges only when entire neighborhoods of external wrenches are included in the stance analysis. We also described experiments where a 2-legged prototype standing on a v-shaped terrain was subjected to disturbance wrenches which varied in a rectangular neighborhood. The experiments showed close matching of the onset of contact rolling and sliding with Coulomb's friction law predictions. Finally, we established that in three dimensions the feasible equilibrium region associated with the nominal gravitational wrench is a convex vertical prism, and sketched some of the challenges involved in its computation.

Let us now discuss extensions of this research. First consider extension of the results to three dimensions. The nominal equilibrium region of a k-contact stance is a convex vertical prism whose cross-section is a semi-algebraic set bounded by high degree polynomials. Once the challenges involved in its computation are resolved, one needs to obtain the robust equilibrium region associated with wrench neighborhoods centered on the gravitational wrench. We also seek a practical approximation for the robust equilibrium region similar to the classical support polygon principle, which is valid only for horizontal flat terrains. A longer term issue is the

construction of locomotion planners based on robust equilibrium regions. While it is tempting to demonstrate the utility of such planners, some caution must be exercised since posture robustness must be augmented with the stability considerations as follows.

The stability of a feasible equilibrium stance consists of two components. First, rigid-body dynamics can be ambiguous in multiple frictional contacts settings (Dupont and Yamajako 1994; Lotstedt 1981; Mason and Wang 1988). Hence one must ensure that a feasible equilibrium stance is non-ambiguous (Lynch 1992) or *strongly stable* (Balkcom and Trinkle 2002, Pang and Trinkle 2000). This condition requires that among all possible static/roll/slip/break reactions at the contacts, static equilibrium is the only dynamically feasible reaction. Second, one must account for classical dynamic stability under small position-and-velocity perturbations. Here, too, one encounters a complication: the mechanics of friction dictates convergence to some nearby zero-velocity stance rather than the original equilibrium stance. Moreover, perturbations that involve contact breakage give rise to collisions having frictional impacts (Chatterjee and Ruina 1998; Stewart 2000; Wang and Mason 1987). The issues of strongness and dynamic stability must be resolved before we attempt to deploy robust postures in practical quasistatic locomotion planner.

Appendix A: Proof Details

This appendix contains proofs of two results stated in Section 2. The first result asserts that $\mathcal{R}(\boldsymbol{w})$ can be computed as the convex hull of the pairwise feasible equilibrium regions.

PROPOSITION 1. Let $\mathcal{B}$ be supported by k frictional contacts in a two-dimensional gravitational environment, and be subjected to an external wrench $\boldsymbol{w} = (f_{ext}, \tau_{ext})$. Then $\mathcal{R}(\boldsymbol{w})$ is the convex hull of the pairwise feasible equilibrium regions,

$$\mathcal{R}(\boldsymbol{w}) = \mathsf{conv}\{\mathcal{R}_{ij}(\boldsymbol{w}),\ 1 \le i, j \le k\},$$

where $\mathcal{R}_{ij}(\boldsymbol{w})$ is the feasible equilibrium region associated with two contacts x_i and x_j, and conv denotes convex hull.

Proof. Let $\tilde{\mathcal{R}}(\boldsymbol{w}) = \mathsf{conv}\{\mathcal{R}_{ij}(\boldsymbol{w}),\ 1 \le i, j \le k\}$. First we show that $\tilde{\mathcal{R}}(\boldsymbol{w}) \subseteq \mathcal{R}(\boldsymbol{w})$, then we show that $\mathcal{R}(\boldsymbol{w}) \subseteq \tilde{\mathcal{R}}(\boldsymbol{w})$.

1. Let $x \in \tilde{\mathcal{R}}(\boldsymbol{w})$. Then there exist center-of-mass locations $x_{ij} \in \mathcal{R}_{ij}(\boldsymbol{w})$ and non-negative scalars λ_{ij} such that $x = \sum_{i,j} \lambda_{ij} x_{ij}$ where $\sum_{i,j} \lambda_{ij} = 1$. Consider now those (i, j) indices for which $\lambda_{ij} \neq 0$. Since $x_{ij} \in \mathcal{R}_{ij}(\boldsymbol{w})$, there exists a $2k$-vector $\boldsymbol{f}_{ij} \ge \vec{0}$ whose only non-zero components are associated with f_i and f_j, such that $\boldsymbol{f}_{ij}$ satisfies the equilibrium condition: $G_f \boldsymbol{f}_{ij} = -f_{ext}$ and $G_\tau \boldsymbol{f}_{ij} = -(x_{ij}^T J^T f_{ext} + \tau_{ext})$. If one chooses the contact forces as $\boldsymbol{f} = \sum_{i,j} \lambda_{ij} \boldsymbol{f}_{ij} \ge \vec{0}$, one gets

$$G_f \boldsymbol{f} = \sum_{i,j} \lambda_{ij} G_f \boldsymbol{f}_{ij} = -\sum_{i,j} \lambda_{ij} f_{ext} = -f_{ext}$$

$$G_\tau \boldsymbol{f} = \sum_{i,j} \lambda_{ij} G_\tau \boldsymbol{f}_{ij} = -\sum_{i,j} \lambda_{ij} (x_{ij}^T J^T f_{ext} + \tau_{ext})$$

$$= -(x^T J^T f_{ext} + \tau_{ext}).$$

Thus $\boldsymbol{f}$ satisfies the equilibrium condition (1) with center of mass at x. Hence $x \in \mathcal{R}(\boldsymbol{w})$.

2. Let $x \in \mathcal{R}(\boldsymbol{w})$. Let τ_{min} and τ_{max} be the solutions of the LP problems (3), and let $\boldsymbol{f}_{min}$ and $\boldsymbol{f}_{max}$ be the values of $\boldsymbol{f}$ corresponding to τ_{min} and τ_{max}. Since x lies in the strip $\mathcal{R}(\boldsymbol{w}) = \{x :\ \tau_{min} \le x \cdot J^T f_{ext} + \tau_{ext} \le \tau_{max}\}$, there exist two center-of-mass locations x_{min} and x_{max} on the edges of $\mathcal{R}(\boldsymbol{w})$ such that $x = \lambda x_{min} + (1-\lambda) x_{max}$ for some $\lambda \in [0, 1]$. Now recall that the extrema of a linear program always include a vertex of the constraints polytope. Let $\mathcal{P}$ denote the constraints polytope. According to (3), $\mathcal{P}$ is given by $\mathcal{P} = \{\boldsymbol{f} \in I\!R^{2k} : G_f \boldsymbol{f} = -f_{ext}, \boldsymbol{f} \ge \vec{0}\}$. Thus $\mathcal{P}$ is defined by two equalities and $2k$ inequalities in $I\!R^{2k}$. Each vertex of $\mathcal{P}$ is an intersection of $2k$ facets of $\mathcal{P}$, hence it satisfies $2k$ equalities out of the $2k+2$ equations: $\boldsymbol{f} = \vec{0}$ and $G_f \boldsymbol{f}_v = -f_{ext}$. As a result, a vertex of $\mathcal{P}$ has at most two non-zero components. Since τ_{min} and τ_{max} are extrema of (3), $\boldsymbol{f}_{min}$ and $\boldsymbol{f}_{max}$ are vertices of $\mathcal{P}$. Focusing first on $\boldsymbol{f}_{min}$, it has at most two non-zero components, say i and j. It follows that $\boldsymbol{f}_{min}$ is generated only by two contact forces at x_i and x_j. But $\boldsymbol{f}_{min}$ corresponds to x_{min} and satisfies $G_f \boldsymbol{f}_{min} = -f_{ext}$ and $G_\tau \boldsymbol{f}_{min} = -\tau_{min} = -(x_{min}^T J^T f_{ext} + \tau_{ext})$. Therefore $x_{min} \in \mathcal{R}_{ij}(\boldsymbol{w})$. Using similar arguments for $\boldsymbol{f}_{max}$, there exist two indices m and n such that $x_{max} \in \mathcal{R}_{mn}(\boldsymbol{w})$. Finally, $x = \lambda x_{min} + (1-\lambda) x_{max}$ and therefore $x \in \mathsf{conv}\{\mathcal{R}_{ij}(\boldsymbol{w}), \mathcal{R}_{mn}(\boldsymbol{w})\} \subseteq \tilde{\mathcal{R}}(\boldsymbol{w})$. □

Corollary 1 immediately follows from the proof of the proposition. There exist at most four distinct contacts x_i, x_j, x_m, x_n such that $\mathcal{R}(\boldsymbol{w}) = \mathsf{conv}\{\mathcal{R}_{ij}(\boldsymbol{w}), \mathcal{R}_{mn}(\boldsymbol{w})\}$. Hence the entire region $\mathcal{R}(\boldsymbol{w})$ is determined by at most four contacts.

Appendix B: Line Sweep Algorithm for Computing $\mathcal{R}(\boldsymbol{w})$

We describe an algorithm for computing the feasible equilibrium strip of a k-contact stance such that $\mathcal{B}$ is subjected to the nominal gravitational wrench $\boldsymbol{w}_0 = (f_g, 0)$ (the algorithm is basically unchanged for a general external wrench). Let e denote the vertical upward direction in the two-dimensional environment, and let (s, t) denote the horizontal and vertical coordinates of the fixed world frame. For simplicity of the

algorithm, we make a reasonable assumption that the friction cones are *upward pointing*, in the sense that $f_i \cdot e \geq 0$ for all $f_i \in \mathcal{C}_i$ and $i = 1 \ldots k$. The algorithm uses two lists $\mathcal{L}_1$ and $\mathcal{L}_2$ for the $2k$ directed lines aligned with the edges of the friction cones. The lines pointing to the *left* of e are stored in $\mathcal{L}_1$, and the lines pointing to the *right* of e are stored in $\mathcal{L}_2$. It is worth noting that the two edges of a particular friction cone can be both left-pointing or right-pointing, e.g. the edges of $\mathcal{C}_2$ in Figure 8(a). The j^{th} line has the form: $l_j = \{(s,t) : t = a_j s + b_j\}$, where (a_j, b_j) are the line's slope and t-axis intercept. Let $\mathcal{S}$ be the set of intersection points of lines in $\mathcal{L}_1$ with the lines in $\mathcal{L}_2$. A key observation is that the edges of $\mathcal{R}(\boldsymbol{w}_0)$ are vertical lines that pass through the leftmost and rightmost points of $\mathcal{S}$. Hence the computation of $\mathcal{R}(\boldsymbol{w}_0)$ reduces to the computation of the leftmost and rightmost points of $\mathcal{S}$. We describe the portion of the algorithm that computes the rightmost point of $\mathcal{S}$.

The following discussion refers to the pseudo-code given below. In step 1.1 the algorithm computes a vertical line $l'(0)$ which lies on the right side of $\mathcal{S}$. The computation of this line is based on a trigonometric formula involving the slope and intercept of the lines in $\mathcal{L}_1$ and $\mathcal{L}_2$ (Or and Rimon 2005). The resulting line $l'(0)$ satisfies the following *separation condition.* Let p_1 denote the highest intersection point of the lines of $\mathcal{L}_1$ with $l'(0)$, and let p_2 denote the lowest intersection point of the lines of $\mathcal{L}_2$ with $l'(0)$. Then $l'(0)$ satisfies the condition that p_2 lies *above* p_1, a condition which implies that $l'(0)$ lies to the right of $\mathcal{S}$ (Figure 8(a). In step 1.2 the algorithm computes an initial vertical sweep line $l(0)$ which passes through a point of $\mathcal{S}$. While any point of $\mathcal{S}$ can be selected, the algorithm selects the intersection point of the highest right-pointing line with the lowest left-pointing line along $l'(0)$ as a good initial guess (Figure 4(a)). Note that $l(0)$ typically does not satisfy the separation condition.

The i^{th} iteration of the algorithm consists of three steps. In step 2.1 the algorithm sets a vertical line at the middle of the strip bounded by $l(i)$ and $l'(i)$. In step 2.2 the algorithm checks the separation condition along the middle line. If it is satisfied, the middle line lies to the right of $\mathcal{S}$ and $l'(i+1)$ moves to the middle line. In this case $l(i+1)$ moves to a new point of $\mathcal{S}$ which lies on the right side of $l(i)$. If the separation condition does not hold on the middle line, $l(i+1)$ moves to a point of $\mathcal{S}$ on the right side of the middle line while $l'(i+1) = l'(i)$. In step 2.3 the algorithm prunes the lists $\mathcal{L}_1$ and $\mathcal{L}_2$ according to their intersection pattern with the new sweep line. Any line in $\mathcal{L}_1$ whose intersection with $l(i+1)$ lies at or above p_2 does not contribute points to $\mathcal{S}$ on the right side of $l(i+1)$. Hence this line is removed from $\mathcal{L}_1$. Similarly, any line in $\mathcal{L}_2$ whose intersection with $l(i+1)$ lies at or below p_1 is removed from $\mathcal{L}_2$. The algorithm terminates when $\mathcal{L}_1$ and $\mathcal{L}_2$ both become empty. This event occurs precisely when $l(i+1)$ passes through the rightmost point of $\mathcal{S}$. A pseudo-code of the algorithm follows.

Line Sweep Algorithm for Computing $\mathcal{R}(\boldsymbol{w}_0)$

Data structures: Lists $\mathcal{L}_1$ and $\mathcal{L}_2$ containing indices of left and right pointing lines.

1. Initialization

1.1 Compute initial vertical line $l'(0)$ on the right side of $\mathcal{S}$:
Set $a^1_{min} = \min_{j\in\mathcal{L}_1} a_j$ and $a^1_{max} = \max_{j\in\mathcal{L}_1} a_j$.
Set $a^2_{min} = \min_{j\in\mathcal{L}_2} a_j$ and $a^2_{max} = \max_{j\in\mathcal{L}_2} a_j$.
Set $b^1_{max} = \max_{j\in\mathcal{L}_1} b_j$ and $b^2_{min} = \min_{j\in\mathcal{L}_2} b_j$.
Set $l'(0)$ at $s'(0) = \max\{\frac{b^1_{max}-b^2_{min}}{a^2_{min}-a^1_{max}}, \frac{b^1_{max}-b^2_{min}}{a^2_{max}-a^1_{min}}\}$.

1.2 Compute initial sweep line $l(0)$:
Set $j'_0 = \arg\max_{j\in\mathcal{L}_1}\{a_j s'(0) + b_j\}$ and $j_0 = \arg\min_{j\in\mathcal{L}_2}\{a_j s'(0) + b_j\}$.
Set $l(0)$ at $s(0) = \frac{b_{j'_0} - b_{j_0}}{a_{j_0} - a_{j'_0}}$.

1.3 Set $i = 0$.

2. Repeat:

2.1 Set middle line at $s_m = (s(0) + s'(0)/2$.

2.2 Check separation condition along middle line:
Set $t^1_{max} = \max_{j\in\mathcal{L}_1}\{a_j s_m + b_j\}$ and $t^2_{min} = \min_{j\in\mathcal{L}_2}\{a_j s_m + b_j\}$.
If $t^2_{min} \leq t^1_{max}$ set $l(i+1)$ at $s(i+1) = s_m$. Goto step 2.3.
Otherwise set $l'(i+1)$ at s_m and $s(i+1) = s(i)$ (middle line lies on right side of $\mathcal{S}$).

2.3 Prune redundant lines from $\mathcal{L}_1$ and $\mathcal{L}_2$:
Set $t^1_{max} = \max_{j\in\mathcal{L}_1} a_j s(i+1) + b_j$ and $t^2_{min} = \min_{j\in\mathcal{L}_2} a_j s(i+1) + b_j$.
Remove from $\mathcal{L}_1$ any j such that $a_j s(i+1) + b_j \leq t^2_{min}$.
Remove from $\mathcal{L}_2$ any j such that $a_j s(i+1) + b_j \geq t^1_{max}$.

2.4 If $\mathcal{L}_1$ and $\mathcal{L}_2$ become empty, return $l(i+1)$ and STOP.

2.5 Move sweep line to a new point of S:
Set $j_0 = \arg\min_{j\in\mathcal{L}_2}\{a_j s(i+1) + b_j\}$.
Set $l(i+1)$ at $s(i+1) = \max_{j\in\mathcal{L}_1} \frac{b_j - b_{j_0}}{a_{j_0} - a_j}$.

2.6 Increment i.

End of repeat loop

The correctness and runtime of the algorithm is summarized in the following lemma. In the lemma, Δ is basically the maximal horizontal distance between the points of $\mathcal{S}$, while δ is bounded from below by the horizontal distance between the two rightmost points of $\mathcal{S}$ (Or and Rimon 2005).

LEMMA 3. (Or and Rimon 2005) Let $\mathcal{B}$ be supported by k upward-pointing frictional contacts and be subjected to the gravitational wrench $\boldsymbol{w}_0 = (f_g, 0)$. Then the sweep line algorithm computes the right edge of $\mathcal{R}(\boldsymbol{w}_0)$ in $O(k \cdot \min\{k, \log(\Delta/\delta)\})$ steps, where Δ is the initial search width and δ is the minimal search width.

In the worst case the algorithm runs in $O(k^2)$ steps, which is the same as a naive computation of all points in $\mathcal{S}$. However, the algorithm repeatedly prunes lines from $\mathcal{L}_1$ and

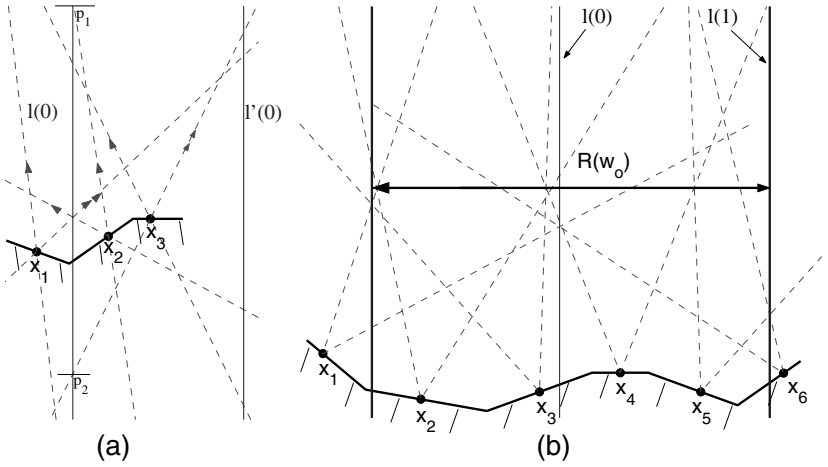

Fig. 8. (a) Illustration of the separation condition (right-pointing lines are double arrowed). (b) Execution of the algorithm on a 6-contact stance.

$\mathcal{L}_2$ and is therefore more efficient than the naive computation. Moreover, in practical settings $\log(\Delta/\delta)$ is a small constant. For instance, let l_0 be the horizontal distance between x_1 and x_6 in the 6-contact stance of Figure 8(b). Then $\Delta = 0.86l_0$, $\delta = 0.06l_0$, and consequently $\log(\Delta/\delta) = 3.85$. Thus $\min\{k, \log(\Delta/\delta)\} = \log(\Delta/\delta)$ in practice, and the time complexity of the algorithm is practically linear in k.

Execution Example: Consider the 6-contact stance shown in Figure 8(b), with a coefficient of friction $\mu = 0.4$. An execution of the algorithm on this example yields the initial sweep line $l(0)$. After the first iteration the sweep line moves to $l(1)$. At this stage the lists $\mathcal{L}_1$ and $\mathcal{L}_2$ become empty and the algorithm terminates with $l(1)$ as the right edge of $\mathcal{R}(\boldsymbol{w}_0)$. Note that a naive computation would require inspection of $6^2 = 36$ intersection points.

References

Balkcom, D. J., Gottlieb, E. J., and Trinkle, J. C. 2002. A sensorless insertion strategy for rigid planar parts.*IEEE International Conference on Robotics and Automation*, pp. 882–887.

Bicchi, A. 2000. Hands for dexterous manipulation and robust grasping: A difficult road toward simplicity. *IEEE Transactions on Robotics and Automation* 16(6):652–662.

Bretl, T., Latombe, J.C., and Rock, S. 2003. Toward autonomous free-climbing robots. *Proceedings of International Symposium on Robotics Research (ISRR)*, 2003.

Bretl, T., Rock, S., and Latombe, J.C. 2003. Motion planning for a three-limbed climbing robot in vertical natural terrain. In *IEEE International Conference on Robotics and Automation*, pp. 2946–2953.

Brost, R. C. 1991. *Analysis and Planning of Planar Manipulation Tasks*. PhD thesis, CMU.

Chatterjee, A. and Ruina, A. 1998. A new algebraic rigid body collision law based on impulse space considerations. *Journal of Applied Mechanics* 65(4):939–951.

Dupont, P. E. and Yamajako, S. P. 1994. Jamming and wedging in constrained rigid-body dynamics. *IEEE International Conference on Robotics and Automation*, pp. 2349–2354.

Erdmann, M. A. 1998. An exploration of nonprehensile two-palm manipulation. *The International Journal of Robotics Research* 17(5):485–503.

Fen, F., Shoham, M., and Longman, R. 1996. Lyapunov stability of force-controlled grasps with a multifingered hand. *The International Journal of Robotics Research* 15(2):137–154.

Ghasempoor, A. and Sepehri, N. 1995. A measure of machine stability for moving base manipulators.*IEEE International Conference on Robotics and Automation*, pp. 2249–2254.

Greenfield, A., Rizzi, A., and Choset, H. 2005. Dynamic ambiguities in frictional rigid-body systems with application to climbing via bracing.*IEEE International Conference on Robotics and Automation*, pp. 1959–1964.

Harada, K., Kajita, S., Kaneko, K K., and Hirukawa, H. 2003. ZMP analysis for arm/leg coordination. *IEEE/RSJ Conference on Intelligent Robots and Systems (IROS)*, pp. 75–81.

Hirai, K., Hirose, M., Haikawa, Y., and Takenaka, T. 1998. The development of Honda humanoid robot. *IEEE International Conference on Robotics and Automation*, pp. 1321–1326.

Kriegman, D. J. 1994. Capture regions of curved 3D objects. *IEEE International Conference on Robotics and Automation*, pp. 595–601.

Kuffner, J., Nishiwaki, K., Kagami, S., Inaba, M., and Inoue, H. 2001. Motion planning for humanoid robots under obstacle and dynamic balance constraints. *IEEE International Conference on Robotics and Automation*, pp. 692–698.

Liu, G. F., Li, J., and Li, Z. X. 2002. Coordinated manipulation of objects by multifingered robotic hand in contact space and active joint space. *IEEE International Conference on Robotics and Automation*, pp. 3743–3748.

Lotstedt, P. 1981. Coulomb friction in two-dimensional rigid body systems. *Zeitschrift fur Angewandte Mathematik und Mechanik* 61:605–615.

Lynch, K. M. and Mason, M. T. 1996. Stable pushing: Mechanics, controllability, and planning. *The International Journal of Robotics Research* 15(6):533–556.

Lynch, K.M. 1992. The mechanics of fine manipulation by pushing. *IEEE International Conference on Robotics and Automation*, pp. 2269–2276.

Madhani, A. and Dubowsky, S. 1992. Motion planning of mobile multi-limb robotic systems subject to force and friction constraints. *IEEE International Conference on Robotics and Automation*, pp. 233–239.

Marhefka, D. W. and Orin, D. E. 1997. Gait planning for energy efficiency in walking machines. *IEEE International Conference on Robotics and Automation*, pp. 474–480.

Mason, M. T. 1991. Two graphical methods for planar contact problems. *IEEE/RSJ Conference on Intelligent Robots and Systems (IROS)*, pp. 443–448.

Mason, M. T. and Wang, Y. 1988. On the inconsistency of rigid-body frictional planar mechanics. *IEEE International Conference on Robotics and Automation*, pp. 524–528.

Mason, R., Burdick, J. W., and Rimon, E. 1997. Stable poses of 3-dimensional objects. *IEEE International Conference on Robotics and Automation*, pp. 391–398.

Mason, R., Rimon, E., and Burdick, J. W. 1995. The stability of heavy objects with multiple contacts. *IEEE International Conference on Robotics and Automation*, pp. 439–445.

McGhee, R. B. and Frank, A. A. 1968. On the stability properties of quadruped creeping gaits. *Mathematical Biosciences* 3(3/4):331–351.

Mirza, K. and Orin, D. E. 1994. General formulation for force distribution in power grasps. *IEEE International Conference on Robotics and Automation*, pp. 880–887.

Nguyen, V.-D. 1988. Constructing force-closure grasps. *The International Journal of Robotics Research* 7(3):3–16.

Omata, T. and Tsukagoshi, K., and Mori, O. 2002. Whole quadruped manipulation. *IEEE International Conference on Robotics and Automation*, pp. 2028–2033.

Omata, T. and Nagata, K. 2000. Rigid body analysis of the indeterminate grasp force in power grasps. *IEEE Transactions on Robotics and Automation*, 16(1):46–54.

Or, Y. and Rimon, E. 2004. Robust multiple contact postures in a two-dimensional gravitational field. *IEEE International Conference on Robotics and Automation*, pp. 4783–4788.

Or, Y. and Rimon, E. 2005. Computation and graphic characterization of robust multiple-contact postures in gravitational environments. Technical report, Dept. Mechanical Engineering, Technion, http://robots.technion.ac.il/publications.

Or, Y. and Rimon, E. 2006. Computing 3-legged equilibrium stances in three-dimensional gravitational environments. *IEEE International Conference on Robotics and Automation*, 2006 (to appear) http://robots.technion.ac.il/publications.

Pang, J. S. and Trinkle, J. C. 2000. Stability characterizations of fixtured rigid bodies with coulomb friction. *IEEE International Conference on Robotics and Automation*, pp. 361–368.

Papadopoulos, E. and Rey, D. 1996. A new measure of tipover stability margin for mobile manipulators. *IEEE International Conference on Robotics and Automation*, pp. 3111–3116.

Rimon, E., Shoval, S., and Shapiro, A. 2001. Design of a spider robot for motion with quasistatic force constraints. *Autonomous Robots*, pp. 279–296.

Schlegl, T., Buss, M., Omata, T., and Schmidt, G. 2001. Fast dextrous regrasping with optimal contact forces and contact sensor-based impedance control. *IEEE International Conference on Robotics and Automation*, pp. 103–108.

Shapiro, A. and Rimon, E. 2003. PCG: a foothold selection algorithm for spider robot locomotion in 2D tunnels. *IEEE International Conference on Robotics and Automation*, pp.2966–2972.

Stewart, D.E. 2000. Rigid-body dynamics with friction and impact. *SIAM Review*, 41(1):3–39.

Trinkle, J. C., Farahat, A. O., and Stiller, P. F. 1995. First-order stability cells of active multi-rigid-body systems. *IEEE Transactions on Robotics and Automation*, 11(4):545–557.

Trinkle, J. C., Farahat, A. O., and Stiller, P. F. 1994. Second-order stability cells of a frictionless rigid body grasped by rigid fingers. *IEEE International Conference on Robotics and Automation*, pp. 2815–2821.

Vukobratovic, M. and Borovac, B. 2004. Zero moment point — thirty five years of its life. *International Journal of Humanoid Robotics*, 1(1):157–173.

Wang, M. Y. 2001. A full-kinematics model of fixtures for precision locating applications. *IEEE/RSJ International Conference on Intelligent Robots and Systems (IROS)*, pp. 1135–1140.

Wang, Y. and Mason, M. T. 1987. Modeling impact dynamics for robotic operations. *IEEE International Conference on Robotics and Automation*, pp. 678–685.

Xu, J. J., Liu, G. F., and Li, Z. X. 2004. On quality functions for grasp synthesis and fixture planning. *IEEE International Conference on Robotics and Automation*, pp. 333–338.

Yokokohji, Y., Nomoto, S., and Yoshikawa, T. 2002. Static evaluation of humanoid robot postures constrained to the surrounding environment through their limbs. *IEEE International Conference on Robotics and Automation*, pp. 1856–1863.

Yoshikawa, T. 1999. Passive and active closure by constraining mechanisms. *Journal of Dynamic Systems, Measurement, and Control* 121(3-4):418–424.